Kinesin Facilitates Phenotypic Targeting of Therapeutic Resistance in Advanced Prostate Cancer

Maddison Archer[1], Diane Begemann[1,2], Edgar Gonzalez-Kozlova[3,4], Prerna R. Nepali[1], Estefania Labanca[5], Peter Shepherd[5], Navneet Dogra[4,6], Nora Navone[5,†], and Natasha Kyprianou[1,3,6]

ABSTRACT

Understanding the mechanisms underlying resistance is critical to improving therapeutic outcomes in patients with metastatic castration–resistant prostate cancer. Previous work showed that dynamic interconversions between epithelial–mesenchymal transition to mesenchymal–epithelial transition defines the phenotypic landscape of prostate tumors, as a potential driver of the emergence of therapeutic resistance. In this study, we use *in vitro* and *in vivo* preclinical MDA PCa patient-derived xenograft models of resistant human prostate cancer to determine molecular mechanisms of cross-resistance between antiandrogen therapy and taxane chemotherapy, underlying the therapeutically resistant phenotype. Transcriptomic profiling revealed that resistant and sensitive prostate cancer C4-2B cells have a unique differential gene signature response to cabazitaxel. Gene pathway analysis showed that sensitive cells exhibit an increase in DNA damage, while resistant cells express genes associated with protein regulation in response to cabazitaxel. The patient-derived xenograft model specimens are from patients who have metastatic lethal castration–resistant prostate cancer, treated with androgen deprivation therapy, antiandrogens, and chemotherapy including second-line taxane chemotherapy, cabazitaxel. Immunohistochemistry revealed high expression of E-cadherin and low expression of vimentin resulting in redifferentiation toward an epithelial phenotype. Furthermore, the mitotic kinesin-related protein involved in microtubule binding and the SLCO1B3 transporter (implicated in cabazitaxel intracellular transport) are associated with resistance in these prostate tumors. Combinational targeting of kinesins (ispinesib) with cabazitaxel was more effective than single monotherapies in inducing cell death in resistant prostate tumors.

Implications: Our findings are of translational significance in identifying kinesin as a novel target of cross-resistance toward enhancing therapeutic vulnerability and improved clinical outcomes in patients with advanced prostate cancer.

Introduction

Prostate cancer, the most common malignancy among men, has favorable survival rates in local disease and early detection (1). The lethality of prostate cancer arises from progression to metastatic disease, resulting in one in 33 American men with prostate cancer succumbing to the disease. Those with metastatic prostate cancer have a 70% chance of mortality within 5 years, largely because of the emergence of treatment resistance and tumor recurrence (1). Second-generation antiandrogens enzalutamide and abiraterone acetate target androgen signaling by preventing the binding of 5α-dihydrotestosterone (DHT) to the androgen receptor (AR) and subsequent translocation to the nucleus and inhibiting the biosynthesis of DHT respectively (2, 3). Androgen deprivation therapy (ADT) and AR signaling inhibitors offer survival benefits in metastatic castration–resistant prostate cancer patients. The majority of prostate cancer patients treated with ADT eventually develop castration-resistant prostate cancer (CRPC) that ultimately recurs and progresses to lethal disease. These therapies have survival benefits for patients with CRPC; however, there is often progression to resistant disease, no longer responsive to antiandrogen therapy (4, 5). At this stage, the only therapeutic strategies that confer improvement in patient survival are first-line taxane chemotherapy and second-line taxane chemotherapy (docetaxel and cabazitaxel), and the recently FDA-approved PARP inhibitors (olaparib; refs. 6–8).

The primary mechanism of antitumor action by taxane chemotherapy proceeds via induction of G_2-M cell cycle arrest and apoptosis in prostate cancer through stabilization of microtubules by binding to β-tubulin and preventing de-polymerization of microtubules, consequentially blocking mitosis (7). Further evidence (from our group) first showed that taxane chemotherapy prevents the translocation of AR to the nucleus, impairing AR signaling and transcriptional activity (9). Cabazitaxel was also shown to have a differential effect as a result of targeting expression of HSET (*KIFC1*), a kinesin protein involved in microtubule binding, assembly of the mitotic spindle and potentially associated with AR (10, 11). This is of major clinical significance, as HSET expression has been linked to therapeutic resistance and poor clinical outcomes in prostate cancer (12). There is potential therapeutic value in targeting HSET to overcome resistance, as *in vitro* studies have shown the resensitization of docetaxel-resistant prostate cancer cells and apoptosis when treated with an HSET inhibitor CW069 (13). Our *In vivo* studies have shown

[1]Department of Urology, Icahn School of Medicine at Mount Sinai, New York, New York. [2]Department of Toxicology and Cancer Biology, University of Kentucky College of Medicine, Lexington, Kentucky. [3]Department of Oncological Sciences, Icahn School of Medicine at Mount Sinai, New York, New York. [4]Department of Genomic Sciences, Icahn School of Medicine at Mount Sinai, New York, New York. [5]Department of GU Medical Oncology, MD Anderson Cancer Center, Houston, Texas. [6]Department of Pathology and Molecular and Cell Based Medicine, Icahn School of Medicine at Mount Sinai, New York, New York.

[†]Deceased

Corresponding Author: Natasha Kyprianou, Department of Urology, 6th Floor, 1425 Madison Avenue, Icahn School of Medicine at Mount Sinai, New York, NY 10029. E-mail: natasha.kyprianou@mountsinai.org

Mol Cancer Res 2024;22:730–45

doi: 10.1158/1541-7786.MCR-23-1047

effective targeting of HSET by treating mice with cabazitaxel therapy following ADT, showing the potential value for sequencing strategies to improve patient clinical response (10).

Prostate tumors acquire a more invasive and stem-like phenotype through the process of epithelial–mesenchymal transition (EMT) leading to the development of metastases and therapeutic resistance (14). This process is characterized by the loss of epithelial markers such as E-cadherin, insulin-like growth factor binding protein 3 (IGFBP3), and their tight junctions, and the upregulation of mesenchymal markers including vimentin (15–17). Previous studies from our group showed that cabazitaxel treatment contributes to the phenotypic reprogramming of prostate cancer cells within the tumor microenvironment, by reversing EMT to mesenchymal–epithelial transition (MET; ref. 11). The cell plasticity that drives interconversion between EMT and MET not only defines the phenotypic landscape of prostate tumors but has also been linked to the emergence of therapeutic resistance and recurrent tumors, yet it provides a potential therapeutic vulnerability window where cells are primed for therapy (17–19). In this study, we profiled the effectors involved in phenotypic redifferentiation in models of therapeutic resistance in prostate cancer, toward the development of a gene signature that underpins the molecular landscape of resistance for potential leads to overcome tumor recurrence and lethal disease.

Materials and Methods

Cell lines

Human prostate cancer cell lines, 22RV1 (CRPC), LNCaP (androgen sensitive), and PC3 (androgen-independent, AR-negative) were obtained from the ATCC (CRL2505, CRL1740, and CRL1435, respectively). Therapeutically resistant human prostate cancer cell lines were generated according to and generously provided by Dr. Allen Gao (University of California, Davis) as previously described, C4-2BER (enzalutamide resistant), C4-2BAR (abiraterone resistant), C4-2BDR (docetaxel resistant), and C4-2B (parental; refs. 20, 21). Cells were maintained using RPMI 1640 (Corning) supplemented with 10% FBS (Thermo Fisher Scientific) and 1% penicillin–streptomycin (Thermo Fisher Scientific) in a 37°C incubator with 5% CO_2. Experiments using DHT-supplemented media with charcoal-stripped FBS (Thermo Fisher Scientific). PC3-CR (cabazitaxel resistant) cell lines were generated through an incremental increase in exposure to cabazitaxel, starting with 0.5 nmol/L, over a 2-month period. Cells were tested for mycoplasma contamination using the ATCC Universal Mycoplasma Detection Kit (30-1012K, ATCC).

Drugs

Antiandrogen drugs enzalutamide and abiraterone were obtained from Selleck Chemicals and Sigma Aldrich, respectively. Both drugs were reconstituted to 10-mmol/L stocks in DMSO and stored at −80°C. Docetaxel obtained from Sigma Aldrich was dissolved in DMSO to 1-mmol/L stocks. Cabazitaxel (CBZ; Sigma Aldrich), dissolved in 100% ethanol and stored at −20°C in 1-mmol/L stocks. Kinesin inhibitors CW069 and ispinesib were purchased from Selleck Chemicals and Sigma Aldrich, respectively.

Cell viability

Cell viability was assessed using the thiazolyl blue tetrazolium bromide (MTT) assay. Cells (5×10^4 cells/mL) at 60% to 70% confluence in 96-well plates were exposed to the respective drugs, enzalutamide (10 μmol/L), abiraterone (10 μmol/L), or docetaxel (50 nmol/L) for 24 and 48 hours. Experiments investigating the effects of cabazitaxel (1–50 nmol/L) or Ispinesib (1–50 nmol/L) on cell viability were exposed to treatment for 24, 48, 72, and 96 hours. Cells were subsequently treated with 1 mg/mL of MTT (Thermo Fisher Scientific) for 1 hour at 37°C and formazan crystals were solubilized with DMSO. Absorbance was measured at 570 nmol/L using SpectraMaxx M5 spectrophotometer (Molecular Devices). All treatments were given in triplicate, and results were presented as the average of three independent experiments.

Cell migration

Cell lines were seeded in six-well plates in triplicate at a density of 2×10^5 cells/well, grown to 60% density. The cell monolayer was wounded with a 10-μL pipette tip. Following wounding, cells were exposed to enzalutamide (10 μmol/L), abiraterone (10 μmol/L), or docetaxel (50 nmol/L). At 24 and 48 hours, images were captured (10× magnification), and the number of cells migrating into the wound was counted in three fields per well. This experiment was replicated three times.

Cell invasion

The invasive potential of therapeutically resistant cell lines was investigated using the matrigel invasion assay. Cells were seeded into the upper chamber of the Biocoat Matrigel Transwell Chamber (Becton Dickinson) at a density of 50,000 cells/well. Non-invasive cells were removed using medium-soaked cotton swabs after 24 and 48 hours, and cells were fixed and stained using the Diff-Quick staining solutions (IMEB, Inc.). Images were captured at 10× magnification, and the number of invading cells was counted in four fields.

Western blot analysis

Total cellular protein was isolated from cell lysates using RIPA buffer (Thermo Fisher Scientific) with protease inhibitor (Thermo Fisher Scientific). Protein concentration of cell lysates was determined using the Pierce BCA Protein Assay Kit (Thermo Fisher Scientific). Proteins were subjected to SDS-PAGE using 10% to 12% SDS-polyacrylamide gels (Bio-Rad) and transferred to polyvinylidene fluoride membranes (Bio-Rad). Membranes were probed with primary antibodies overnight at 4°C followed by exposure to species-specific horseradish peroxidase–labeled secondary antibodies (Cell Signaling Technology). Probes were detected with WesternBright ECL spray (Advansta) and visualized using GE ImageQuant chemiluminescence. GAPDH was used as a loading control.

In vivo xenograft experiments

All animal experiments were performed according to the Institutional Animal Care and Use Committee Office of Animal Care Use and Welfare at the Icahn School of Medicine at Mount Sinai. Six to eight weeks old male NOD-*scid* gamma mice (The Jackson Laboratory) were injected subcutaneously into right flank with C4-2B or C4-2BDR cells (5 million in 100-μL media) mixed with 100 μL Matrigel (Corning). After 4 weeks, tumors reached a palpable size and were treated with cabazitaxel at 3 mg/kg every 3 days for 2 weeks, the vehicle control groups were administered 1:1:18 vol/vol of ethanol: polysorbate 80: 5% wt/vol glucose in sterile water. Treatments were administered via intraperitoneal injection. Tumors were measured every 3 days and tumor volume was calculated by

length × width × 0.5236. Three days after the final treatment, mice were euthanized using CO_2 according to approved guidelines, and tumors were existed for analysis. One mouse was excluded from the analysis due to significant toxicity from cabazitaxel.

Coimmunoprecipitation

Cells were lysed using the Pierce IP Lysis buffer (Thermo Fisher Scientific). Coimmunoprecipitation was performed using the Dynabeads Protein G Kit according to the manufacturer's instructions with cross-linking with the Pierce BS^3 Crosslinker (Thermo Fisher Scientific). Anti-KIFC1 and Anti-Bcl2 Antibodies were used at 5 μg/sample. Antibodies used are summarized in Supplementary Table S1.

RNA sequencing

RNA sequencing (RNA-seq) of PC3 and PC3-CR cells was done using the Human Clariom-S array analysis with the assistance of the University of Kentucky Microarray Core Facility. Total RNA was extracted from prostate cancer cells using TRIzol reagent (Invitrogen/Life Technologies) and the recommended protocol for RNA isolation. RNA-seq of C4-2B samples was performed at the Genetic and Genomics Core Facilities at Icahn School of Medicine at Mount Sinai. We used 50-bp single-end and 30 million reads per sample for a total of 18 samples. Illumina Stranded mRNA library prep kit was used to prepare the RNA material for sequencing. NextSeq 500/550 High output (75 cycles) was utilized to amplify the mRNAs. Briefly, the resulting reads were quality-controlled using FASTQC, MultiQC, and SamTools. The reads were aligned to Human Genomic Reference HG38 with splicing sensitive aligner STAR 2.7. Gene counts were quantified using FeatureCounts. Downstream differential expression analysis and pathway enrichment were performed using R packages Dream, mle4, VariancePartition, enrichR, and GSVA, and figures were generated with ggplot2, tidyverse complexheatmap, and pheatmap packages. Data are available upon request.

Quantitative RT-PCR analysis

Total RNA was extracted using PureLink RNA Mini Kit (Invitrogen) according to the manufacturer's instructions. One microgram of RNA sample was subjected to reverse transcription using the iScript cDNA synthesis kit (Bio-Rad). Quantitative real-time RT-PCR was performed in the CFX96 Real-Time Detection System (Bio-Rad) with Sybr green-based detection using specific primers for *CBLN2*, *NECTIN3*, *LRG1*, *ELF5 TRIM2*, *KIF5C*, *MARCKS*, *WLS*, *Snail*, *Slug*, *Zeb1*, and *Twist1* (Thermo Fisher Scientific). Each PCR reaction included three technical replicates, data represents the average of three repeated independent experiments, normalized to Actin expression (ΔΔCT) and expressed relative to untreated controls.

Transporter siRNA silencing

For gene silencing in prostate cancer cells, the shRNA vector was obtained from Open Biosystems. After transfection, the shRNA SLCO1B3 transporter gene in LNCaP cells was selected using puromycin (a resistance marker). Polyclonal populations were pooled under antibiotic selection media and after several passages, stable cell lines were characterized as previously described (22).

IHC analysis of PDX specimens

Formalin-fixed, paraffin-embedded tissue specimens from patient-derived xenograft model (PDX) sections (5 μm) of male patients with advanced CRPC were provided by Dr. Nora Navone (MD Anderson Cancer Center) as part of the MDA PCa PDX series as previously described (23). Sections were subjected to IHC analysis using antibodies against E-cadherin, vimentin, cytokeratin 18, HSET, B-cell lymphoma-2 (Bcl-2), and solute carrier organic anion transporter family 1B3 (SLCO1B3; the antibodies used are summarized in Supplementary Table S1). Slides were de-paraffinized, rehydrated, and heat-induced antigen retrieval was performed using the Dako antigen retrieval solution at 100°C. Sections were exposed to primary antibodies overnight at 4°C, followed by detection with IHC-select species–specific biotinylated secondary antibodies and horseradish peroxidase–streptavidin (Millipore). Visualized was achieved using 3′3-diaminobenzidine chromogen substrate kit (Dako). Images were captured using a NanoZoomer digital scanner (Hamamatsu Photonics). The positively stained HSET (nuclear) was quantified at 40× magnification by two independent observers each in three random fields.

Statistical analysis

Numerical assay data were analyzed via one- or two-way ANOVA to test for statistical significance between cell lines and treatments using GraphPad Prism 9. PC3 data were analyzed using a Student *t* test. Data are expressed as mean ± standard error of the mean. Statistical significance was inferred when $P < 0.05$. RNA-seq data were normalized and modeled using mixed effect models for precise modeling of time points and the two cellular conditions (resistant and sensitive). RNA-seq quality control using count distribution, library size, and gene detection of at least five counts between samples was performed to remove potential sequencing artifacts. Differential expression tests part of mixed effect models used moderate t statistics. Hierarchical clustering was performed using the R package HMISC implementing the "ward.D2" method (24). Pathway enrichment analysis was done using local enrichR to survey all available gene set databases with a focus on gene ontology and MsigBD. Pathways were ranked based on the number of genes per pathway, odds ratio, and false discovery rate-adjusted *P*-values. All *P*-values were adjusted using multiple testing adjustments (25).

Data availability

Data processing and analysis scripts are deposited at https://github.com/eegk and available upon request. All other relevant data that support the conclusions of the study are within the supplementary material or available from the authors upon request.

Results

Characterization of cross-resistance to antiandrogens and first-line taxane chemotherapy

We determined the response of human prostate cancer cell lines that are resistant to enzalutamide (C4-2BER), abiraterone (C4-2BAR), and docetaxel (C4-2BDR), to antiandrogens and docetaxel chemotherapy, based on cell viability assessment in response enzalutamide (10 μmol/L), abiraterone (10 μmol/L), and docetaxel (50 nmol/L). Docetaxel induced significant cell death, as identified by the significant reduction in cell viability in response to the drug at 24 and 48 hours of treatment ($P < 0.05$), except for the docetaxel-resistant C4-2BDR (**Fig. 1A** and **B**). At 24 hours, 22RV1 cells (CRPC) exhibited partial sensitivity in response to docetaxel and the antiandrogen abiraterone by 48 hours of treatment (**Fig. 1A** and **B**). The C4-2B cells showed a significant loss of cell viability in response to both antiandrogens and docetaxel. The enzalutamide-resistant C4-

2BER and abiraterone-resistant C4-2BAR failed to show a cell death induction after treatment (24 hours) to either antiandrogen. However, by 48 hours, C4-2BER showed sensitivity to abiraterone, and C4-2BAR exhibited differential response to all drugs (**Fig. 1A** and **B**). The taxane-resistant C4-2BDR cells failed to respond to any of the drugs at 24 hours (**Fig. 1A** and **B**). We also examined the effect of antiandrogen on prostate cancer cell migration (**Fig. 1G** and **H**; Supplementary Fig. S1A). 22RV1 cells showed minimal migration, while C4-2B parental cells showed the highest migration potential at 24 and 48 hours. Treatment with enzalutamide or abiraterone did not affect the migration of 22RV1, C4-2B, C4-2BER, and C4-2BAR. Only in response to abiraterone, there was a significant reduction in cell migration of C4-2BDR cells ($P < 0.05$; **Fig. 1G** and **H**).

The invasive potential of resistant cell lines was investigated using matrigel invasion assays. All cell lines showed invading cells at 24 and 48 hours (**Fig. 1D–F**). At 24 hours, the resistant cell lines showed no difference in the number of invading cells compared with the C4-2B cells (**Fig. 1D** and **E**). At 48 hours, the enzalutamide-resistant C4-2BER had a significantly greater number of invading cells compared with C4-2B and C4-BDR (**Fig. 1D** and **E**).

Phenotypic profiling of the effectors of cross-resistance by Western blot revealed that IGFBP3 is upregulated in C4-2BDR cells compared with C4-2B cells (24 hours). Both antiandrogen-resistant cell lines exhibited similar protein expression profiles, while Bcl-2 expression was downregulated in response to docetaxel in both cell lines. HSET expression is induced by docetaxel in parental and antiandrogen-resistant cells and not targeted as observed with cabazitaxel (**Fig. 1C**; ref. 11).

Phenotypic interconversions drive cross-resistance to cabazitaxel

A time course and dose response to cabazitaxel were investigated in C4-2B cell models; our findings showed that docetaxel-resistant C4-2BDR cells exhibit significant cross-resistance to cabazitaxel (**Fig. 2A–D**). At 48 hours, C4-2BDR have significantly greater viability when exposed to 1 to 35 nmol/L of cabazitaxel compared with parental cells (**Fig. 2B**). In concentrations up to 10 nmol/L, C4-2BDR cells maintain greater than 50% cell viability through 96 hours. At higher doses (50 nmol/L), there is no difference in response to cabazitaxel (**Fig. 2A–D**). For subsequent experiments, a dose of 20 nmol/L was used for 48 hours treatment period. At concentrations of cabazitaxel up to 20 nmol/L, C4-2BDR cells showed reduced sensitivity to the drug compared with all other cell lines (Supplementary Fig. S2A–D). Antiandrogen-resistant cell lines C4-2BER and C4-2BAR, and 22RV1 CRPC cells showed similar viability profiles to the parental C4-2B cells. This response was consistent at higher doses of cabazitaxel (35–50 nmol/L; **Fig. 2A–D**; Supplementary Figs. S2 and S3). Early results from *in vivo* xenograft C4-2B and C4-2BDR tumors suggest cabazitaxel is not effective in reducing tumor growth in C4-2BDR tumors compared with C4-2B tumors and vehicle controls (Supplementary Fig. S3H and I).

The phenotypic profile of this cross-resistance to cabazitaxel was analyzed via Western blot (20 nmol/L; 0–48 hours). E-cadherin was consistently upregulated when exposed to cabazitaxel for 12 to 48 hours, and IGFBP3 was increased in C4-2BDR-resistant cells. This suggests that cabazitaxel is driving an interconversion between EMT and MET in resistant cells. No significant changes were detected in HSET levels in taxane-resistant cells. Bcl-2 expression decreases in response to cabazitaxel treatment (**Fig. 2E**). By co-immunoprecipitation, an interaction between Bcl-2 and HSET was observed, and was enriched when exposed to cabazitaxel for 6 hours (**Fig. 2F**). Expression of genes involved in the regulation of EMT were comparatively analyzed via qRT-PCR in the two cell lines. Expression of *Slug*, *Twist*, and *Zeb1* were upregulated in C42BDR cells in response to cabazitaxel after 9 to 24 hours (**Fig. 2H–J**) but no differences in *Snail* mRNA (**Fig. 2G**).

Tracing genes involved in phenotypic reprogramming and therapeutic resistance

To gain mechanistic insights into the phenotypic landscape that underpins therapeutic resistance, we performed an RNA-seq on C4-2B and C4-2BDR cells, to determine their differential response to cabazitaxel (20 nmol/L, 6–12 hours). Principal component analysis reveals that C42B and C4-2BDR cells have distinct gene profiles during treatment (**Fig. 3A**; Supplementary Figs. S4 and S5). The heat maps depict the significant (FDR < 0.05) gene signature responses of C4-2B (**Fig. 3B**), and C4-2BDR (**Fig. 3C**) to cabazitaxel over time and show the 30 most affected genes (LogFC > 2, FDR < 0.01), though C4-2B cells exhibited a greater number of gene changes in response to cabazitaxel. Differential expression analysis reveals the largest differences in mRNA expression in resistant cells, and response to cabazitaxel (**Fig. 3D** and **E**). Resistant C4-2BDR cells exhibited high expression of *CBLN2*, *ELF5*, *ELOVL5*, *FAM155B*, *GNAQ*, and *GCH1*, downregulation of *LRG1* and *B4GALNT* compared with sensitive C4-2B cells, and expression is maintained following cabazitaxel treatment (**Fig. 3D**). Treatment with cabazitaxel increased expression of *WLS* and *NECTIN3*, while expressions of *SLC16A3*, *COLEC12*, *EPHA3*, and *PDIA2* were reduced compared with C4-2B cells (**Fig. 3E**). In C4-2B cells, treatment with cabazitaxel, led to enhancement/activation of gene pathways involved in autophagy, cell cycle stress, and apoptosis. In the resistant C4-2BDR cells, transcriptomic profiling revealed enrichment of DNA replication and repair pathways in response to taxane. Pathways engaged in stemness and unfolded protein response were enriched in both sensitive and resistant prostate cancer cells after treatment; however, this differential activation was significantly higher in the C4-2BDR-resistant cells (**Fig. 3F**).

To validate the results of RNA-seq, qRT-PCR was completed on C4-2B and C4-2BDR cells after treatment with cabazitaxel (24 hours). Consistent with RNA-seq, the mRNA expression of *CBLN2*, *NECTIN3*, and *ELF5* were upregulated in untreated C4-2BDR cells, and this continued through exposure to cabazitaxel (Supplementary Fig. S6A, B, and F). Expression of *MARCKS* and *TRIM2* was induced by cabazitaxel in C4-2BDR resistant cell lines (Supplementary Fig. S6E and G). *LRG1* and *KIF5C* exhibited reduced expression in C4-2BDR-resistant cells compared with C4-2B parental cells, which continued with cabazitaxel treatment (Supplementary Fig. S6C and D). This was consistent with RNA-seq analysis; however, expression of *WLS* was variable (Supplementary Fig. S6H).

Functional loss of SLCO1B3 to underpin therapeutic resistance

Transcriptomic analysis revealed alterations in solute carrier (SLC) family transport proteins associated with therapeutic resistance. Combined expression of SLC family transporters in C4-2B RNA-seq analysis revealed a global downregulation of these transporters in resistant C4-2BDR cells and reduced expression of transporters with treatment with cabazitaxel in both cell lines (**Fig. 4A** and **B**). To further investigate the role of SLC transporters in prostate cancer cells, androgen-independent PC3 cells were continually exposed to increasing doses of cabazitaxel to develop PC3-CR cells, which exhibit increased cell viability in response to cabazitaxel compared with PC3 cells (**Fig. 4C**). RNA-seq analysis of

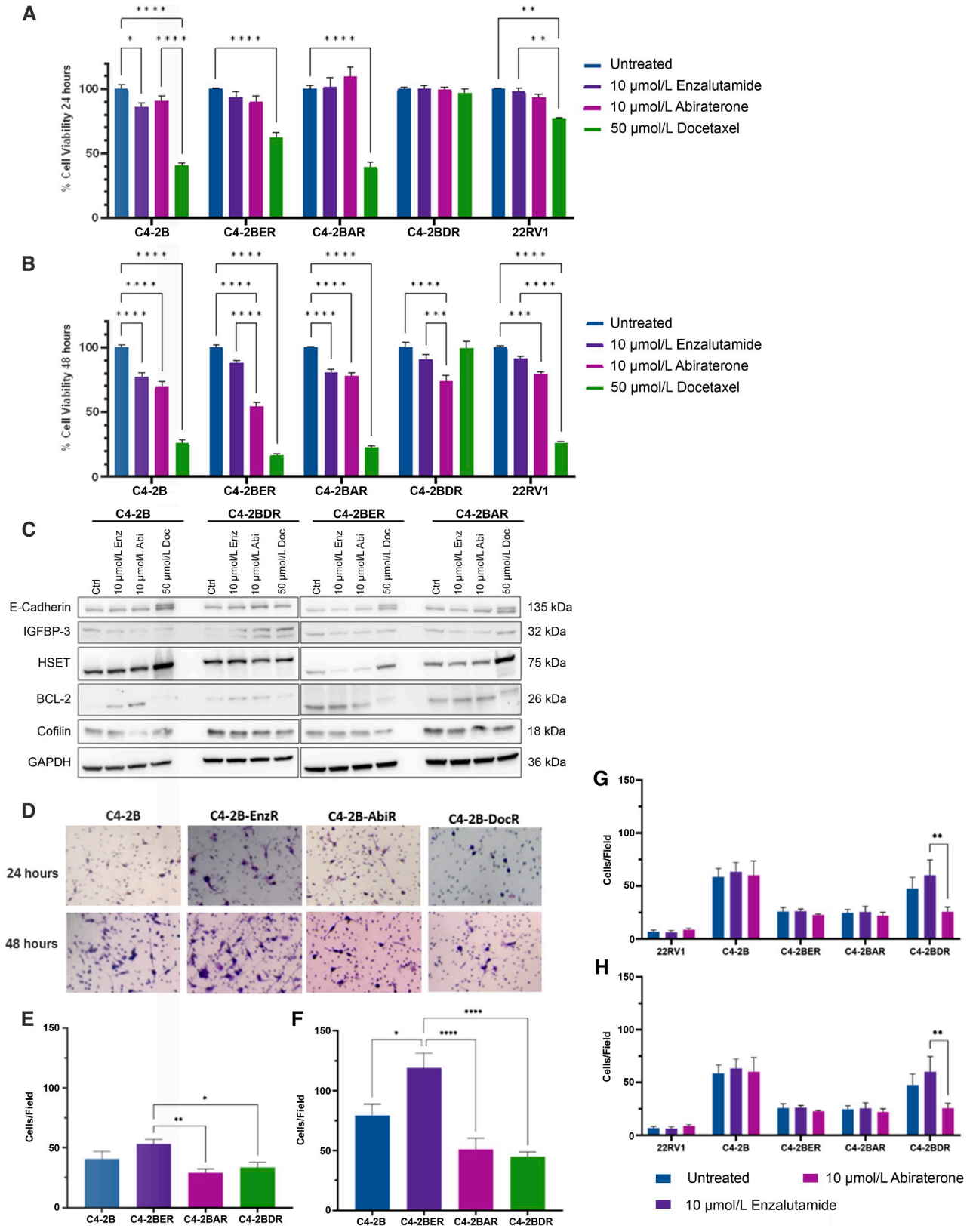

these cells revealed downregulation of the SLC family membrane transporter *SLCO1B3* in the cabazitaxel-resistant prostate cancer cells compared with the PC3 control cells (**Fig. 4D**). This result was validated using qRT-PCR, and loss of SCLO1B3 in PC3-CR cells at a protein level was demonstrated via Western blot (**Fig. 4E** and **F**). To examine the functional contribution of SLCO1B3 to cabazitaxel resistance in PC3 cells, we silenced SLC01B3 expression by shRNA knockdown (a shCONTROL vector and three shSLCO1B3 constructs were selected). Dose–response treatment for a period of 96 hours demonstrated that shSLCO1B3 Clones C and D had greater cell viability in response to increasing doses of cabazitaxel, compared with control and shSLCO1B3-A cells (**Fig. 4G**). In the publicly available clinical prostate cancer database, The Cancer Genome Atlas (TCGA), SCLO1B3 alterations, which were most commonly shallow deletions or deep deletions, were associated with a decrease in progression-free survival, and overall survival (**Fig. 4H**; Supplementary Fig. S8B). IHC analysis for SLCO1B3 in MDA PCa PDX specimens from patients with advanced CRPC showed very little staining, except in PDX derived from Patient 4, derived from circulating tumor cells (Supplementary Fig. S8A).

Phenotypic signatures of lethal prostate cancer MDA PCa PDX models

To investigate the clinical relevance of phenotypic signatures of therapeutic resistance, PDX tumors derived from patients with advanced, treatment-resistant prostate cancer were utilized (MDA PCa PDX). These tumors were all derived from patients with advanced metastatic CRPC that had undergone different treatment sequences and regimes. All patients had received cabazitaxel, except for Patient 1 (donor of MDA PCa 183-A), who is treatment naïve. Eight samples were studied, including four samples (MDA PCa 342-A + B, 350-A + B, 355-9, 355-15) derived from one patient longitudinally (Patient 5a, 5b, 5c, 5d). The clinical characteristics of these tumors are summarized in Supplementary Table S2. The tumors were phenotypically profiled for EMT–MET interconversion, based on E-cadherin and vimentin immunohistochemistry. The PDX from Patient sample 1 (treatment naïve), maintained strong expression of the epithelial marker E-cadherin, with minimal vimentin expression. Interestingly, the PDX from Patient 4, who had undergone cabazitaxel treatment following ADT and abiraterone treatment, exhibited strong expression of E-cadherin and weak vimentin staining. This suggests that treatment reverts to an epithelial phenotype (via MET). Conversely, PDX from Patient 2 and all longitudinal samples derived from Patient 5 (5a–d) appeared mesenchymal in phenotype (based on vimentin and E-cadherin immunostaining, Supplementary Fig. S9).

Since we previously demonstrated sequencing cabazitaxel treatment after ADT *in vivo* reduces the expression of HSET in castration-sensitive prostate cancer xenografts (10), we subsequently investigated the expression of HSET in PDX models of therapeutically resistant prostate cancer and the correlation with the sequencing regimen in the patients (with advanced disease) they were derived from. HSET protein expression was detected in all PDX samples with strong nuclear immunoreactivity (**Fig. 5A**). Models derived from Patients 2 and 3 had the highest level of immunoreactivity (approximately 33%). For PDX from Patient 5, there was variability in HSET expression levels ranging from 15% to 25% of cells expressing HSET. PDX derived from treatment naïve Patient 1 had low expression of HSET, with 10% positively stained cells. PDX from Patient 4 exhibited the lowest positivity for HSET, only 8% of cells were positively stained (**Fig. 5A** and **B**). This may be a result of treatment sequencing, targeting of HSET by cabazitaxel following antiandrogen therapy. However, RNA-seq analysis of these tumors revealed variable expression of HSET (*KIFC1*) at an mRNA level, with no clear correlation of mRNA level with protein expression (Supplementary Fig. S10D). In publically available TCGA data sets, alterations (most commonly amplification) were associated with decreased disease-free survival, and mRNA expression of HSET is higher in prostate cancer tissues compared with benign disease (**Fig. 5C**; Supplementary Fig. S10E). Concurrently, immunohistochemistry of anti-apoptotic Bcl-2 was performed in these specimens. The highest Bcl-2 immunoreactivity was observed in PDX from Patient 3, which was derived from a lymph node. Patient 4 and all Patient 5 PDX samples displayed Bcl-2 positivity, while PDX from treatment naïve Patient 1, and Patient 2 failed to show any immunoreactivity (**Fig. 5A**).

The AR expression status was also assessed via IHC analysis in serial sections. PDX tumors from two patients exhibited AR positivity, treatment-naïve–derived tumor specimens exhibited strong AR positivity (80% of cell population), and tumors derived from Patient 4 (PDX developed from circulating tumor cells) had 90% AR positivity. Expression of AR mRNA was assessed in these specimens using RNA-seq, PDX from Patients 1 and 4 showed expression of AR consistent with the IHC profile (Supplementary Fig. S10A–C).

Targeting kinesins to overcome resistance

The effect of kinesin inhibition to overcome taxane resistance was interrogated by targeting kinesin proteins. As shown in **Fig. 6A–D**, a dose response of C4-2B and C4-2BDR cell lines to kinesin inhibitor ispinesib revealed that during the treatment period of 24 to 96 hours, the C4-2BDR cells showed resistance to ispinesib in a dose-dependent pattern (5–35 nmol/L). Exposure to a higher dose resulted in a 40% loss of cell viability (vs. the untreated controls). The C4-2B cells exhibited high sensitivity to ispinesib with a 60% cell death when treated with ispinesib (5–50 nmol/L, 24–96 hours; **Fig. 6A–D**). Similar response patterns were observed for other cell lines resistant to enzalutamide or abiraterone (Supplementary Fig. S11). The optimal dose of CW069 was determined using dose response for 24 to 48 hours (Supplementary Fig. S12); 5 nmol/L of ispinesib was used for subsequent experiments. To investigate the combined targeting of kinesins with cabazitaxel and kinesin

Figure 1.

Differential response to antiandrogens and taxane chemotherapy in prostate cancer resistant cell lines. **A** and **B,** show the results of cell viability of C4-2B, C4-2BER, C4-2BAR, and C4-2BDR in response to enzalutamide (10 μmol/L), 10 μmol/L abiraterone or docetaxel (50 nmol/L) at 24 (**A**) and 48 hours (**B**) measured by the MTT assay. **C,** Western blot analysis of E-cadherin, IGFBP3, HSET, BCL2, and cofilin protein levels in response to enzalutamide (10 μmol/L), abiraterone (10 μmol/L), or docetaxel (50 nmol/L; for 24 hours); GAPDH was used as a loading control. **D,** Representative images of the matrigel invasion assay; cells were counted in four fields of view from three independent experiments at 24 (**E**) and 48 (**F**) hours. Following the wound scratch assay, images were taken in three fields of view and quantified at 24 (**G**) and 48 (**H**) hours. Data represent mean of three independent experiments in triplicate ± SEM, *, $P < 0.05$; **, $P < 0.01$; ***, $P < 0.001$; ****, $P < 0.0001$ as determined by two-way ANOVA.

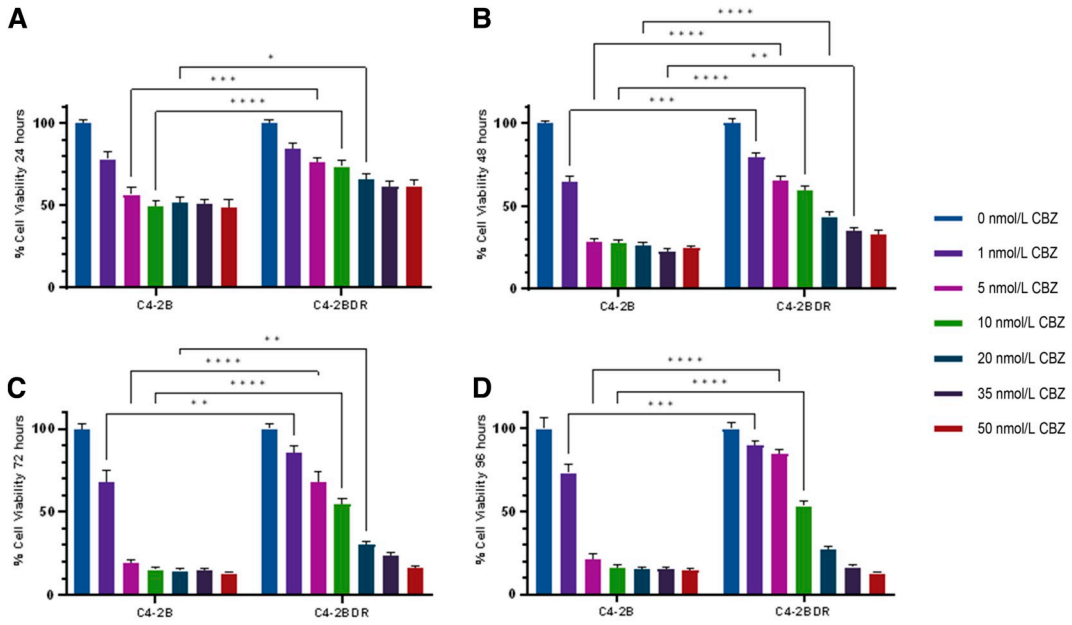

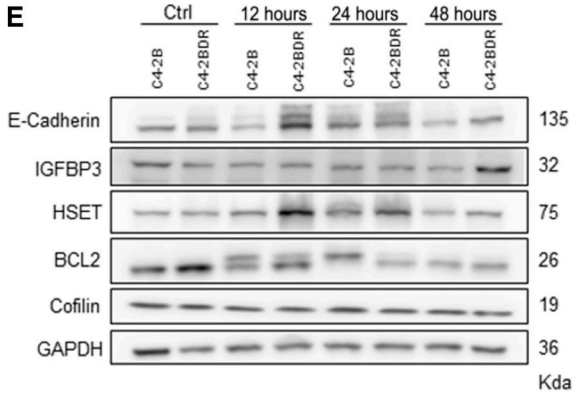

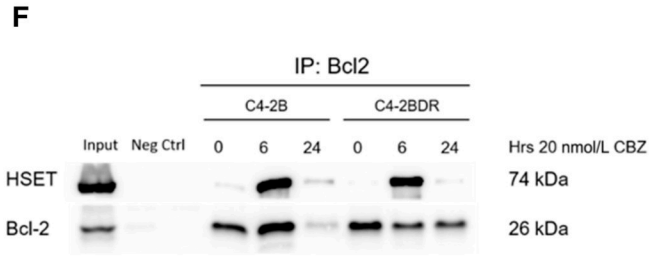

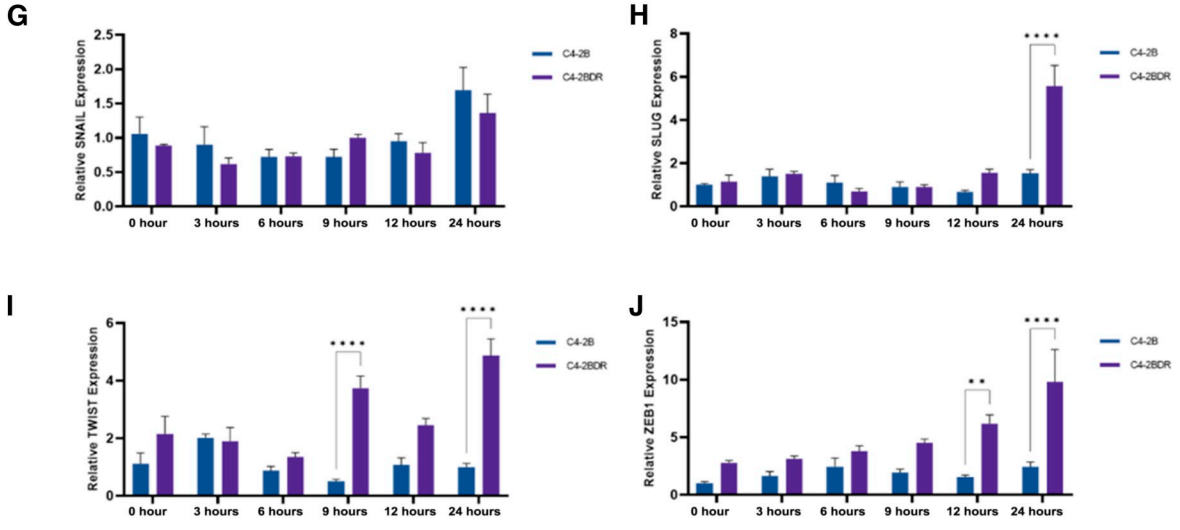

inhibition, we used C4-2B, C4-2BDR, and 22RV1 prostate cancer cells as cell models, treated with cabazitaxel as monotherapy or combination with kinesin or specific HSET inhibitors ispinesib or CW069 for 24 to 48 hours. As shown in **Fig. 6E** and **F**, the combination of ispinesib or CW069 with cabazitaxel caused a significant induction of cell death than any of the drugs given alone (40% after 48 hours). Similarly, there was significant cell death in resistant C4-2BDR prostate cancer cells upon combination treatment of cabazitaxel with CW069 or ispinesib, compared with cabazitaxel alone (**Fig. 6E** and **F**).

Protein profiling of phenotypic effectors (via Western blot) in C4-2B and C4-2BDR cells revealed an increase in the expression of E-cadherin in response to cabazitaxel in combination with ispinesib in sensitive cells. HSET expression peaks at 24 hours of treatment in C4-2B cells after each treatment; however, in C4-2BDR cells expression remains high. Similarly, the expression of anti-apoptotic protein Bcl-2 is high in C4-2BDR cells. In response to ispinesib and cabazitaxel combination treatment, we detected downregulation of Bcl-2 in sensitive, but not in resistant cells (C4-2B-DR; **Fig. 6G**; Supplementary Fig. S13). C4-2B cells exhibited reduced HSET expression when treated with CW069 alone, confirming the specificity of drug targeting. E-cadherin followed a similar pattern in these cells, expression was low with treatment with CW069 but was increased when cabazitaxel was added, this result was also reflected in resistant C4-2BDR cells. HSET expression remained high in C4-2BDR cells and increased at 24 hours with CW069 in combination with cabazitaxel before reducing at 48 hours. Bcl-2 levels remained consistently high in C4-2BDR cells as well as in sensitive C4-2B cells, in response to CW069 treatment. Caspase activation (cleaved caspase 3) was detected in both cell lines after 48 hours of CW069 in combination with cabazitaxel (**Fig. 6H**; Supplementary Fig. S14).

We subsequently examined the phenotypic traits of the resistant prostate cancer C4-2BDR cells in response to kinesin targeting by ispinesib and CW069 by qRT-PCR. Expression of EMT and HSET genes was assessed after combination treatment (with cabazitaxel; 6–24 hours). A compensatory increase effect of CW069 is observed in *KIFC1* expression in both C4-2BDR and parental cells when combined with cabazitaxel. Similarly, *KIFC1* expression is increased in response to ispinesib either as a monotherapy or in combination with cabazitaxel by 24 hours in C4-2B cells and 12 hours in C4-2BDR cells. However, this reduced back to baseline by 24 hours (Supplementary Fig. S15A and B). An increase in *E-cadherin* levels was detected in C4-2B cells at 24 hours of treatment with all drug combinations; however, in the resistant cells, an *E-cadherin* increase was detected in response to a combination of CW069 with cabazitaxel (Supplementary Fig. S15C and D). No significant changes were observed in the transient expression of *Snail* or *Slug* in response to different treatments in either cell line, and variable expression of RNA-seq genes was observed in response to kinesin targeting (Supplementary Figs. S15 and S16).

Targeting HSET-AR interactions triggers phenotypic reprogramming

We recently showed that cabazitaxel targets the association between the kinesin HSET and the AR, which affects the EMT phenotype (10). To gain mechanistic insights into this interaction, the effect inhibiting HSET on transcriptional regulation of EMT was assessed in LNCaP cells. The results shown in **Fig. 7**, indicate the cells treated with CW069 with and without androgens (DHT) in CSS for 6, 12, and 24 hours had *PSA* expression induced by DHT, which was significantly downregulated by HSET inhibition by CW069 (**Fig. 7A**). Expression of *KIFC1* was downregulated by CW069, but restored by DHT administration. However, by 24 hours expression is reduced in both conditions treated with CW069 (**Fig. 7B**). *E-cadherin* expression was markedly increased by CW069 (**Fig. 7C**). This was associated with the expression of *Snail*, a transcriptional repressor of E-cadherin, that was significantly decreased by HSET inhibitor (CW069), regardless of androgens (**Fig. 7D**). At a protein level (by Western blot), HSET expression was dramatically decreased by CW069. Concurrently, PSA was decreased by HSET inhibition by CW069 regardless of the presence of androgens (DHT; **Fig. 7E**).

Discussion

The plasticity of prostate tumors contributes to the heterogeneity and acquisition of therapeutic resistance in advanced prostate cancer (26). Previous work from our lab demonstrated that EMT is induced by transforming growth factor beta (TGFβ) and/or androgens, with a threshold AR level determining the phenotypic outcome and invasive properties (27, 28). Moreover, there is clinical evidence that a switch from E- to N-cadherin expression predicts prostate tumor progression, recurrence, and mortality (29), and therapeutic targeting of N-cadherin in CRPC has emerged as a strategy for blocking metastasis (30, 31).

Previous studies by our group established an interaction between the mitotic spindle kinesin protein HSET and AR that was targetable by sequencing of antiandrogens and cabazitaxel in preclinical models of castration-sensitive prostate cancer but not CRPC (10). In the present study, we provide the first evidence that pharmacologic targeting of kinesins [via HSET specific inhibitor (CW069) and kinesin inhibitor ispinesib] can potentially overcome (therapeutic) taxane resistance to cabazitaxel in cell models of advanced prostate cancer. Evidence on the resensitization of docetaxel-resistant prostate cancer through combinations of CW069 and docetaxel (13), supports our observations. Significantly enough, limited efficacy has been demonstrated in the Southwest Oncology Group phase II clinical trials of kinesin-targeting ispinesib in the treatment of CRPC with docetaxel resistance despite HSET overexpression associated with resistance (12, 32). Further, our observations in androgen-sensitive human prostate cancer LNCaP cells demonstrate reduced PSA expression following HSET inhibition by CW069

Figure 2.

Phenotypic profiling of cross-resistance in docetaxel-resistant prostate cancer cells to cabazitaxel. **A–D,** reveal the dose response of C4-2B and C4-2BDR cells to increasing concentrations (0–50 nmol/L) of cabazitaxel at 24 (**A**), 48 (**B**), 72 (**C**), and 96 hours (**D**). The results represent the mean of three independent MTT assay experiments in triplicate as a percentage of untreated controls. **E,** Western blot analysis of E-cadherin, IGFBP3, HSET, BCL2, and cofilin protein levels in response to 20-nmol/L cabazitaxel in C4-2B and C4-2BDR cells (12–48 hours). GAPDH was used as a loading control; the data are representative of three experiments. **F,** Bcl-2 coimmunoprecipitation of C4-2B and C4-2BDR cells treated with cabazitaxel (12 and 24 hours). **G–J,** C4-2B and C4-2BDR cells were treated with cabazitaxel (20 nmol/L) as indicated, and mRNA was analyzed via RT-PCR for transcriptional regulators of EMT were measured by qRT-PCR; (**G**)-*SNAIL*, (**H**)-*SLUG*, (**I**)-*TWIST*, and (**J**)-*ZEB1*. Data presented as average relative expression to untreated C4-2B cells from three independent experiments performed in triplicate (mean ± SEM, *, $P < 0.05$; **, $P < 0.01$; ***, $P < 0.001$; ****, $P < 0.0001$ by ANOVA).

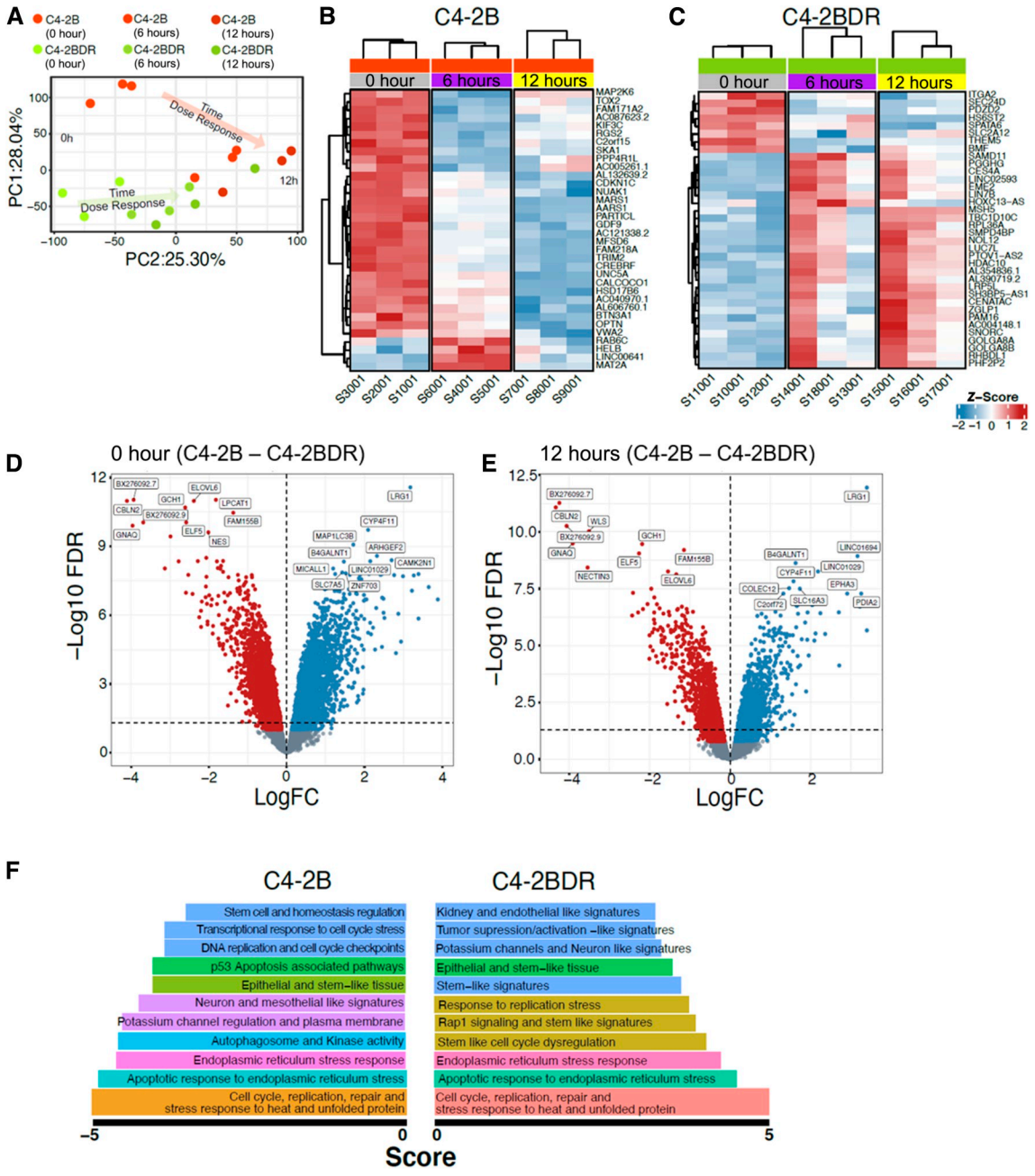

Figure 3.

RNA-seq analysis of differential response of cabazitaxel sensitive and resistant prostate cancer cells. **A,** Principal component analysis between C4-2B and C4-2BDR in response to cabazitaxel (20 nmol/L). **B** and **C,** heat-map of the unique gene signatures after cabazitaxel treatment of C4-2B and C4-2BDR, respectively. Volcano plot between C4-2B and C4-2BDR at 0 hours (**D**) and 12 hours (**E**) cabazitaxel treatment. Top enriched gene pathways in C4-2B and C4-2BDR cells in response to cabazitaxel (**F**).

(regardless of the presence of androgens). This evidence supports the use of combinational strategies before taxane resistance emerges to reduce HSET expression, priming prostate cancer cells for vulnerability to cabazitaxel treatment. Sequencing of cabazitaxel after ADT, effectively targets HSET levels and EMT to MET reversion in PDX models (MDA PCa PDX) of lethal prostate cancer (**Fig. 5A**; Supplementary Fig. S8). Ongoing studies investigate the synergistic combination, as well as temporal sequencing strategies of kinesin inhibition to overcome cabazitaxel resistance using preclinical *in vivo* models of advanced prostate cancer.

The transcriptomic profiling of the response to cabazitaxel in taxane-resistant prostate cancer cells revealed a "global" loss of SLC family transport proteins and cabazitaxel-resistant cells exhibited a loss of SLC protein SLCO1B3. Functional studies further revealed

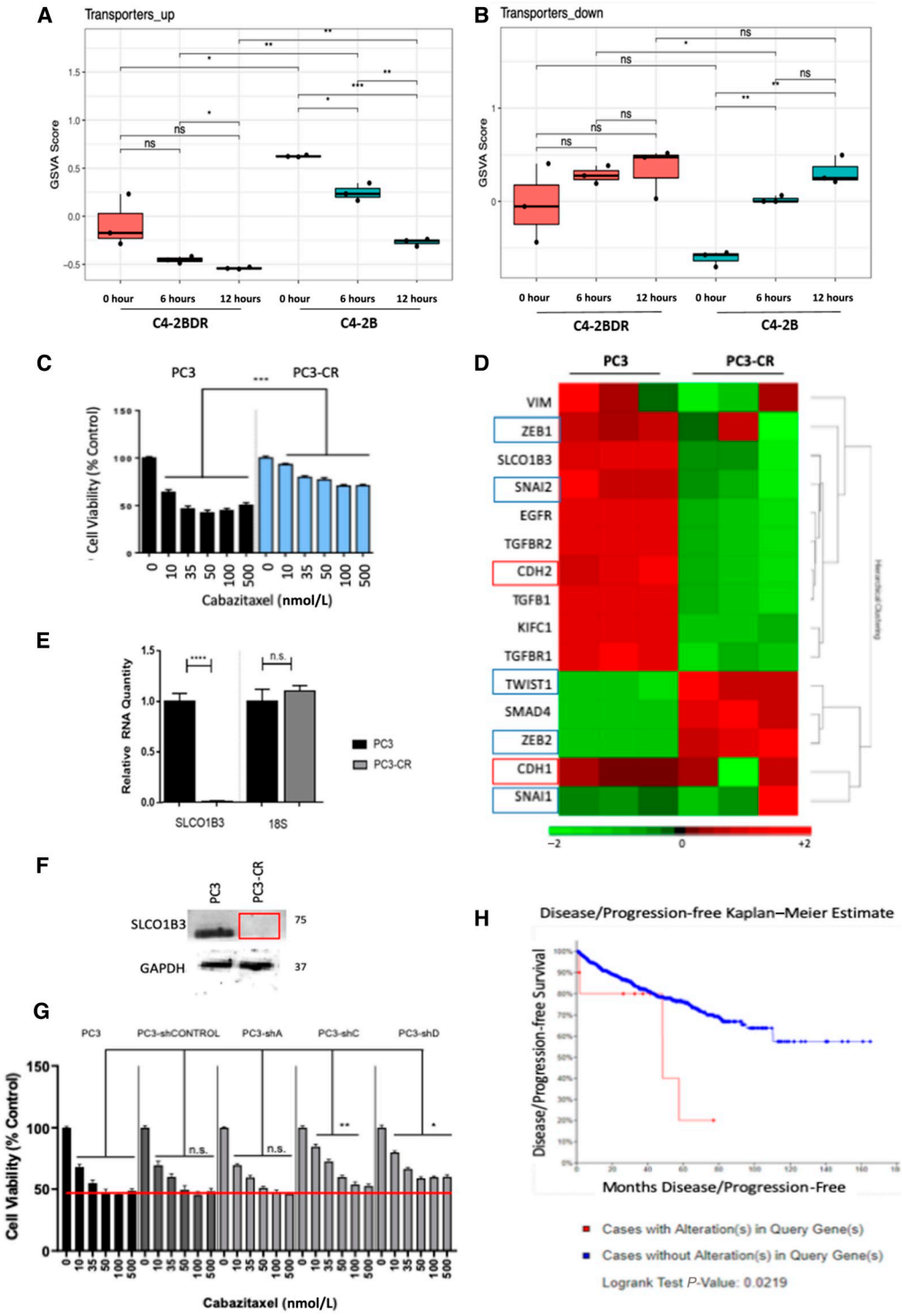

Figure 4.

Loss of SLCO1B3 as a mediator of cabazitaxel resistance. **A** and **B,** RNA-seq expression signatures of SLC family transporter genes in C4-2B (sensitive) and C4-2BDR (resistant) cells after 6 and 12 hours of cabazitaxel treatment. **C,** Dose response of parental PC3 and cabazitaxel-resistant PC3-CR cells to cabazitaxel for 96 hours. **D,** RNA-seq analysis of PC3 and PC3-CR cells. **E** and **F,** expression of SLCO1B3 in PC3 and PC3-CR cells via RT-PCR normalized to 18 seconds (**E**), and Western blot (**F**, GAPDH as loading control). **G,** Cell viability analysis of PC3-shSLCO1B3 stable knockdown in dose response to cabazitaxel. **H,** Kaplan–Meier plot depicts progression-free survival of patients with alterations in the SLCO1B3 gene (red) and no alterations (blue) as determined by the TCGA database. Statistical significance indicated by *, $P < 0.05$; **, $P < 0.01$; ***, $P < 0.001$; ****, $P < 0.0001$; Student *t* test.

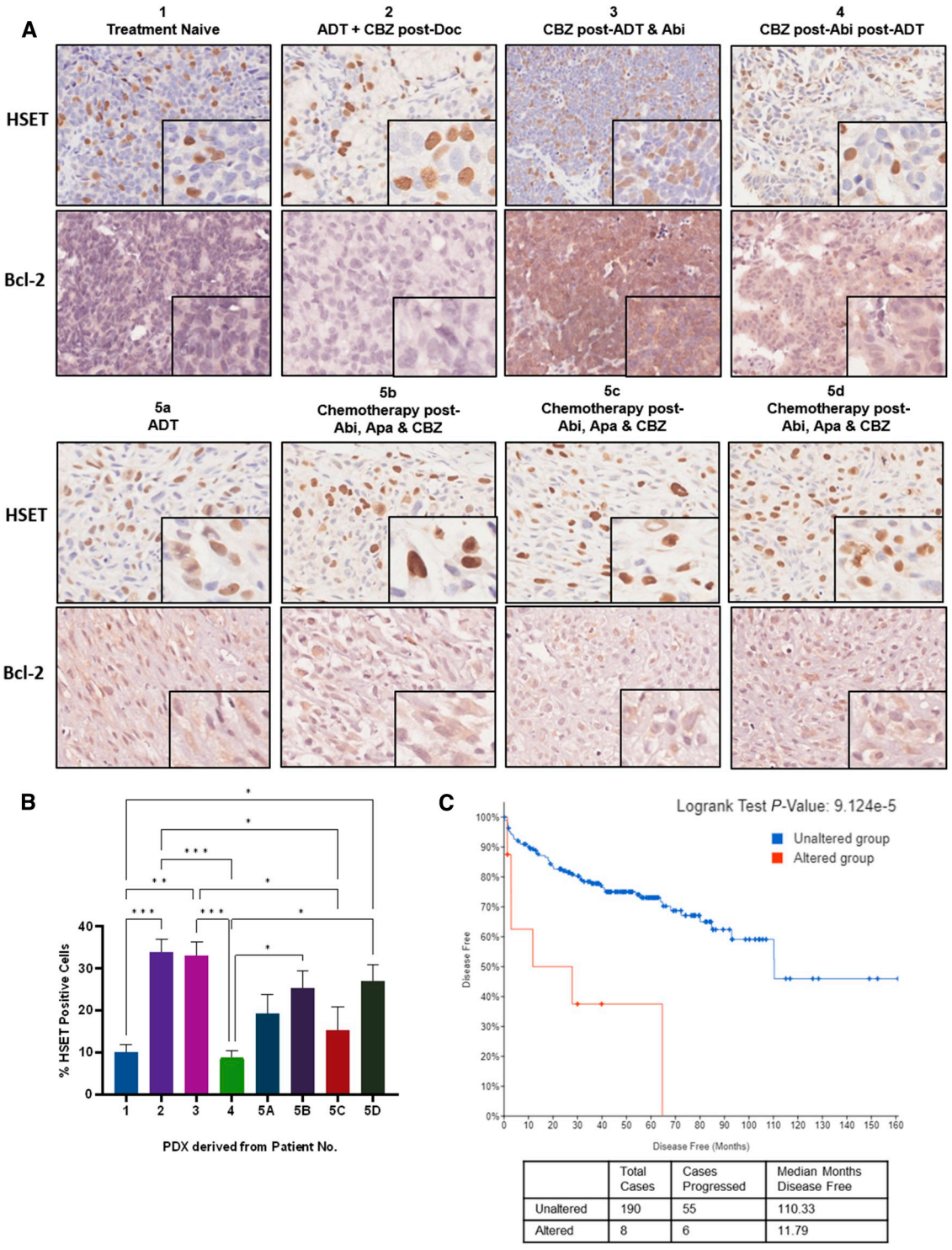

	Total Cases	Cases Progressed	Median Months Disease Free
Unaltered	190	55	110.33
Altered	8	6	11.79

Figure 5.

Profiling of kinesin and survival protein in lethal prostate cancer MDA PCa PDX models. **A,** PDX prostate cancer specimens were subjected to HSET and Bcl-2 immunohistochemistry, shown by representative images at 20× and 40× magnification. **B,** Quantification analysis of HSET immunohistochemistry represented as the mean percentage of positive cells (from six fields of view), analyzed by two independent observers. Statistical significance indicated by *, $P < 0.05$; **, $P < 0.01$; ***, $P < 0.001$; ****, $P < 0.0001$; Student *t* test. **C,** Kaplan–Meier plot depicts progression-free survival of patients with alterations in the HSET gene (red) and no alterations (blue) as determined by the TCGA database.

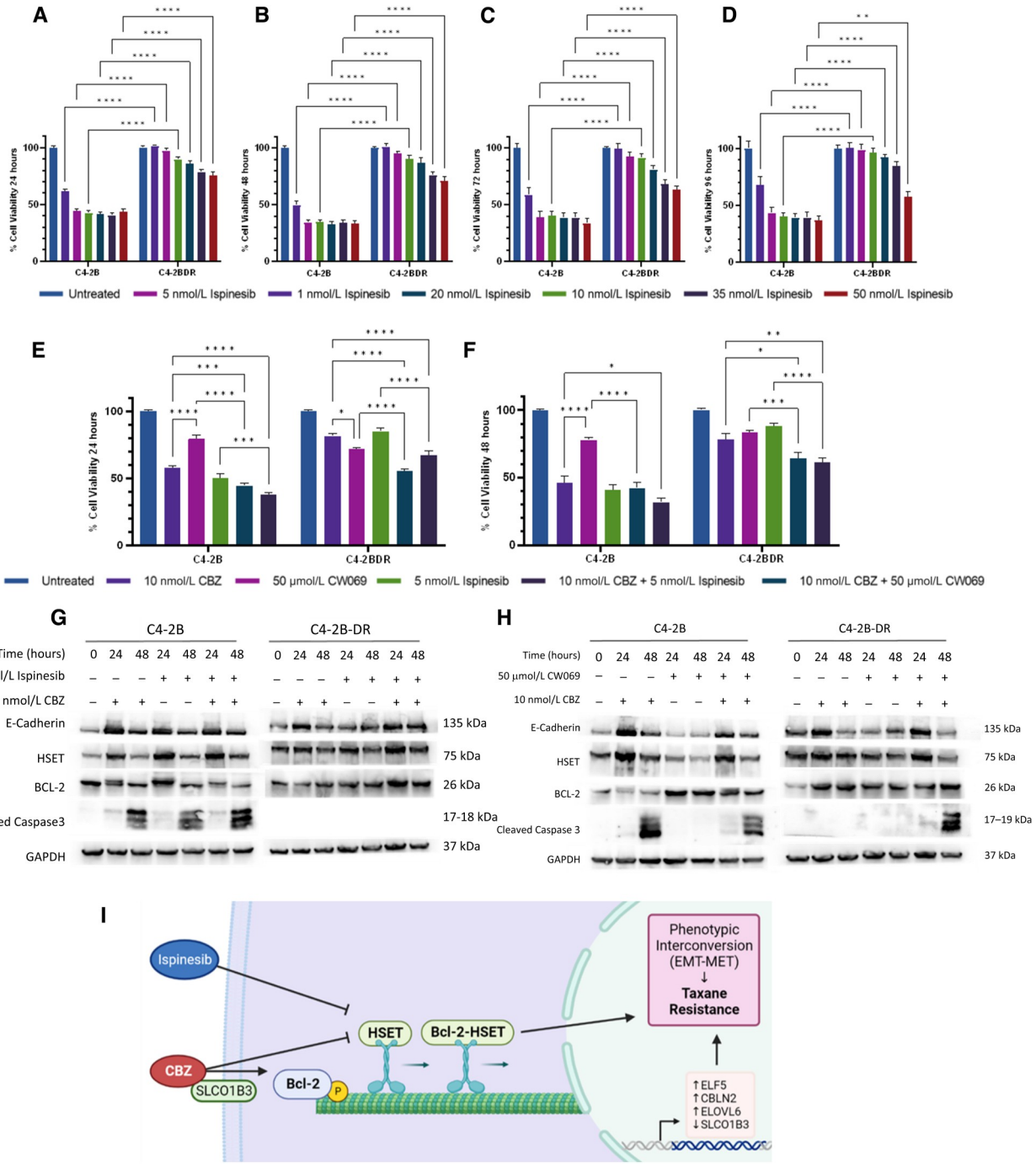

Figure 6.

Combinational targeting of kinesins to overcome therapeutic resistance in prostate cancer cells. Dose response of cell viability of C4-2B and C4-2BDR prostate cancer cells to kinesin inhibitor ispinesib at 24, 48, 72, and 96 hours, respectively shown on (**A–D**); (0–50 nmol/L). C4-2B and C4-2BDR cells were treated with kinesin inhibitors CW069 (50 µmol/L) or ispinesib (5 nmol/L) alone or in combination with cabazitaxel (10 nmol/L) for 24 and 48 hours. Viability was determined by MTT assay after 24 (**E**), and 48 hours (**F**). Data presented as mean ± SEM of three independent experiments in triplicate, expressed as a percentage of untreated controls. Western blot analysis of EMT, HSET, and apoptotic proteins in C4-2B and C4-2BDR cells following treatment with combinations of CW069 (**G**) or ispinesib (**H**) and cabazitaxel. GAPDH was used as a loading control. **I,** Schematic illustration revealing that in taxane-resistant prostate cancer cells, there is upregulation of HSET and Bcl-2 proteins, loss of SLCO1B3 transporter, and increased gene expression of ELF5, CBLN2, and ELOVL6. These key players contribute to the interconversion dynamic between epithelial and mesenchymal phenotypes in response to cabazitaxel. Inhibition of mitotic kinesins (HSET) and survival (Bcl-2) proteins, along with microtubule targeting cabazitaxel provides a potentially powerful platform to overcome therapeutic resistance in CRPC. Statistical significance indicated by *, $P < 0.05$; **, $P < 0.01$; ***, $P < 0.001$; ****, $P < 0.0001$ as determined by two-way ANOVA. (**I,** Created with BioRender.com.)

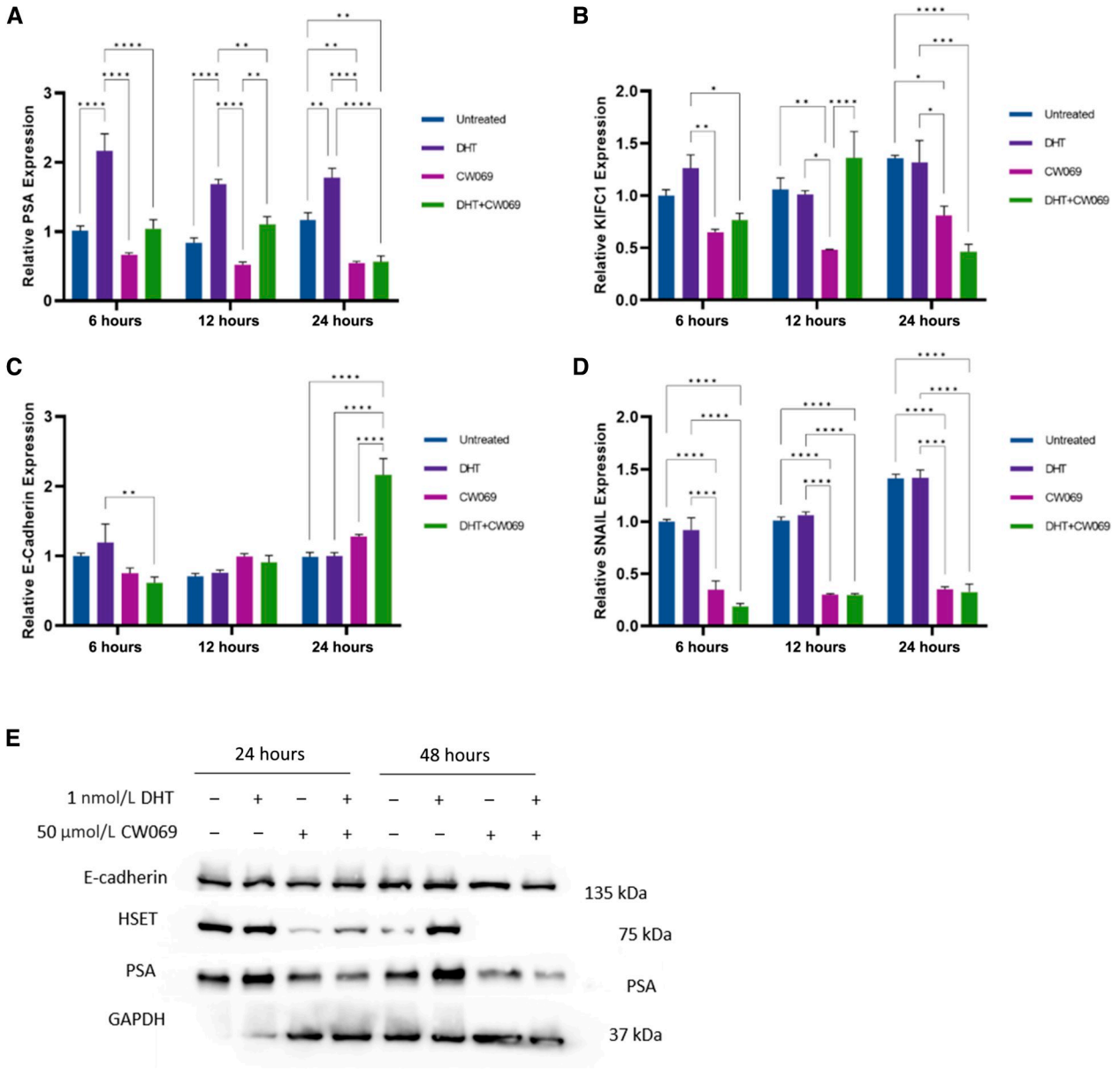

Figure 7.

Transcriptional regulation of EMT by kinesins and androgens. Human prostate cancer cells LNCaP, were treated with 50 µmol/L CW069 (HSET inhibitor) in the presence or absence of DHT (1 nmol/L) for 6, 12, and 24 hours in CSS. RT-PCR was subsequently performed to evaluate the mRNA levels *PSA* (**A**), *KIFC1* (**B**), *E-cadherin* (**C**), and *SNAIL* (**D**). **E,** Data presented as average relative expression to untreated controls from three independent experiments performed in triplicate (mean ± SEM, *, $P < 0.05$; **, $P < 0.01$; ***, $P < 0.001$; ****, $P < 0.0001$).

that silencing SLCO1B3 induced resistance to cabazitaxel. SLCO1B3 plays a role in the influx of taxane chemotherapy into the cells, the loss of SLCO1B3 may lead to less internalization of these drugs, preventing their action on microtubules and thereby mediating tumor recurrence post-taxane treatment. Direct support for our findings stems from recent studies (by other investigators) using docetaxel-resistant PDX models (33, 34), that also demonstrated increased therapeutic vulnerability to taxane treatment upon SLCO1B3 upregulation (34). The SLCO1B3 transporter is functionally engaged in the transport of other taxanes, docetaxel, into cells (33, 35, 36), evidence of clinical significance as in clinical prostate cancer data from the TCGA dataset indicates that deletion/loss of expression of SLCO1B3 is associated with reduced progression-free and overall survival. Mechanistically, the SLC family proteins may mediate resistance and progression to CRPC through drug transport and reprogramming of cellular metabolic pathways (37).

Bcl-2 as a determinant of apoptosis evasion is involved in the emergence of CRPC (38). Topologically Bcl-2 is associated with microtubules (the primary target for taxane chemotherapy), and

becomes functionally inactivated through phosphorylation, resulting in apoptosis (refs. 39–41; **Fig. 6I**). The sustained high expression of Bcl-2 in C4-2BDR cells may suggest driving role for Bcl-2 in taxane resistance; furthermore, an association of Bcl-2 with HSET that is transiently enriched with cabazitaxel treatment was identified here (**Fig. 6I**). Inhibition of Bcl-2 has demonstrated some clinical success in resensitizing tumors to platinum-based therapies and Bcl-2 inhibition by Venetoclax in combination with antiandrogen enzalutamide for the treatment of prostate cancer is currently being trialed (41, 42). However, the function of Bcl-2 and kinesins outside of apoptotic suppression as determinants of phenotypic reprogramming, through the association with microtubules and kinesins warrants further mechanistic pursuit.

Transcriptomic profiling of the response to cabazitaxel in the docetaxel-resistant C4-2B prostate cancer cells revealed that CBLN2 was highly expressed in taxane-resistant cells before and after cabazitaxel treatment. CBLN2 is primarily expressed in the cerebellum and is involved in synaptic cell adhesion maintenance (43). The role of CBLN2 in cancer development is currently unknown; however, increased CBLN2 expression has been detected in cabazitaxel-resistant 22Rv1 xenograft tumors and CRPC clinical samples (44, 45). CBLN2 may be contributing to the increased plasticity pathways in resistant cells, as it has been shown to drive the transition of endothelial cells to mesenchymal phenotype through activation of Twist1 through the NFκB/HIF1α (46). Additionally, our results revealed an upregulation of ELOVL6 associated with taxane resistance in prostate cancer cells. ELOVL family genes play a vital role in fatty acid lipid metabolism, through fatty acid chain elongation, a notable event in cancer cells to meet the metabolic demands of uncontrolled proliferation (47, 48). ELOVL6 is overexpressed in several cancers including breast cancer, lung cancer, and hepatocellular cancer (49–51). While the contribution of ELOVL6 to prostate cancer progression has not yet been fully elucidated, other ELOVL family members (particularly ELOVL5 and ELOVL7) have been implicated in prostate cancer growth and metastasis (52–54). Alterations in fatty acid metabolism by EMT regulator TGFβ suggest a relationship between lipid metabolism and phenotypic reprogramming with targeting potential (55, 56). E74-like transcription factor (ELF5) is consistently upregulated in resistant cell lines and retains high expression following cabazitaxel treatment (**Fig. 6I**). ELF5 is a multifunctional transcription factor that binds AR, expressed by epithelial cells with roles in lineage plasticity determination and EMT (57). In contrast to our findings, there are reports that ELF5 is a repressor of EMT through inhibition of TGFβ signaling by phosphorylation of SMAD3 (58). In this mechanistic context, however, one must also consider the temporal nature of the interconversion between EMT–MET phenotypes. Furthermore, loss of ELF5 expression is associated with prostate cancer progression and enzalutamide resistance, providing a novel functional pursuit of ELF5 in preventing progression to therapeutic resistance (57). There were no changes in genes involved in lineage transitions between basal, luminal, and neuroendocrine phenotypes (TP53/RB1, JAK-STAT, and SOX2; ref. 59).

Epigenetic reprogramming is responsible for silencing tumor-suppressor genes, activating oncogenic drivers, and reprogramming the cistrome of critical transcription factors in prostate cancer as the AR (60, 61). The present study identified kinesins and the SLC family transporters, as new actionable targets that call for further validation. Interrogating the chromatin landscape using an assay for transposase-accessible chromatin with sequencing (ATAC-Seq) in a cohort of clinical prostate specimens (pre- and post-ADT) will provide an informative platform to study the contribution of epigenetic reprogramming to the lethal phenotype and guide clinical making regarding therapeutic intervention and survival outcomes in patients with advanced disease. This work supports the use of combinational strategies of cabazitaxel with targeted inhibitors to mitotic kinesins (HSET) to overcome therapeutic resistance via phenotypic reprogramming within the tumor microenvironment in advanced prostate cancer.

Authors' Disclosures

No disclosures were reported.

Authors' Contributions

M. Archer: Conceptualization, formal analysis, validation, investigation, visualization, methodology, writing–original draft, project administration, writing–review and editing. **D. Begemann:** Formal analysis, validation, investigation, visualization, methodology, writing–review and editing. **E. Gonzalez-Kozlova:** Data curation, formal analysis, investigation, visualization, methodology, writing–review and editing. **P.R. Nepali:** Validation, investigation, methodology, project administration, writing–review and editing. **E. Labanca:** Resources, formal analysis, investigation, visualization, methodology, writing–review and editing. **P. Shepherd:** Resources, formal analysis, investigation, visualization, methodology, writing–review and editing. **N. Dogra:** Data curation, formal analysis, funding acquisition, investigation, visualization, methodology. **N. Navone:** Conceptualization, resources, funding acquisition, investigation, methodology, writing–review and editing. **N. Kyprianou:** Conceptualization, resources, supervision, funding acquisition, methodology, writing–original draft, project administration, writing–review and editing.

Acknowledgments

We would like to acknowledge Yao Shen (Tisch Cancer Institute) for technical assistance with the immunohistochemical analysis and mouse xenograft studies, and Dr. Goutam Chakraborty (Department of Urology, Mount Sinai) for scientific discussions. This work was supported by grants from the National Institutes of Health/NCI, R01 CA232574 (N. Kyprianou), R21 AG078848 (N. Dogra), and P20 CA264076 (N. Dogra). Prostate Cancer Foundation, NCI Cancer Center Support Grant (P30CA16672), Cancer Center Prostate Cancer SPORE (NIH/NCI P50 CA140388), David H. Koch Center for Applied Research in Genitourinary Cancers at MD Anderson (Houston, TX), and NIH/NCI U01 CA224044 (N. Navone).

Note

Supplementary data for this article are available at Molecular Cancer Research Online (http://mcr.aacrjournals.org/).

Received December 15, 2023; revised February 16, 2024; accepted April 16, 2024; published first April 22, 2024.

References

1. Siegel RL, Miller KD, Wagle NS, Jemal A. Cancer statistics, 2023. CA Cancer J Clin 2023;73:17–48.
2. O'Donnell A, Judson I, Dowsett M, Raynaud F, Dearnaley D, Mason M, et al. Hormonal impact of the 17alpha-hydroxylase/C(17,20)-lyase inhibitor abiraterone acetate (CB7630) in patients with prostate cancer. Br J Cancer 2004;90:2317–25.
3. Tran C, Ouk S, Clegg NJ, Chen Y, Watson PA, Arora V, et al. Development of a second-generation antiandrogen for treatment of advanced prostate cancer. Science 2009;324:787–90.
4. Scher HI, Fizazi K, Saad F, Taplin ME, Sternberg CN, Miller K, et al. Increased survival with enzalutamide in prostate cancer after chemotherapy. N Engl J Med 2012;367:1187–97.

5. de Bono JS, Logothetis CJ, Molina A, Fizazi K, North S, Chu L, et al. Abiraterone and increased survival in metastatic prostate cancer. N Engl J Med 2011;364:1995–2005.
6. de Bono J, Mateo J, Fizazi K, Saad F, Shore N, Sandhu S, et al. Olaparib for metastatic castration-resistant prostate cancer. N Engl J Med 2020;382: 2091–102.
7. Huizing MT, Misser VH, Pieters RC, ten Bokkel Huinink WW, Veenhof CH, Vermorken JB, et al. Taxanes: a new class of antitumor agents. Cancer Invest 1995;13:381–404.
8. de Bono JS, Oudard S, Ozguroglu M, Hansen S, Machiels JP, Kocak I, et al. Prednisone plus cabazitaxel or mitoxantrone for metastatic castration-resistant prostate cancer progressing after docetaxel treatment: a randomised open-label trial. Lancet 2010;376:1147–54.
9. Zhu ML, Horbinski CM, Garzotto M, Qian DZ, Beer TM, Kyprianou N. Tubulin-targeting chemotherapy impairs androgen receptor activity in prostate cancer. Cancer Res 2010;70:7992–8002.
10. Begemann D, Wang Y, Yang W, Kyprianou N. Androgens modify therapeutic response to cabazitaxel in models of advanced prostate cancer. Prostate 2020; 80:926–37.
11. Martin SK, Pu H, Penticuff JC, Cao Z, Horbinski C, Kyprianou N. Multinucleation and mesenchymal-to-epithelial transition alleviate resistance to combined cabazitaxel and antiandrogen therapy in advanced prostate cancer. Cancer Res 2016;76:912–26.
12. Sekino Y, Oue N, Shigematsu Y, Ishikawa A, Sakamoto N, Sentani K, et al. KIFC1 induces resistance to docetaxel and is associated with survival of patients with prostate cancer. Urol Oncol 2017;35:31.e13–20.
13. Sekino Y, Oue N, Koike Y, Shigematsu Y, Sakamoto N, Sentani K, et al. KIFC1 inhibitor CW069 induces apoptosis and reverses resistance to docetaxel in prostate cancer. J Clin Med 2019;8:225.
14. Nanda JS, Koganti P, Perri G, Ellis L. Phenotypic plasticity—alternate transcriptional programs driving treatment resistant prostate cancer. Crit Rev Oncog 2022;27:45–60.
15. Huber MA, Kraut N, Beug H. Molecular requirements for epithelial-mesenchymal transition during tumor progression. Curr Opin Cell Biol 2005;17: 548–58.
16. Natsuizaka M, Ohashi S, Wong GS, Ahmadi A, Kalman RA, Budo D, et al. Insulin-like growth factor-binding protein-3 promotes transforming growth factor-{beta}1-mediated epithelial-to-mesenchymal transition and motility in transformed human esophageal cells. Carcinogenesis 2010;31:1344–53.
17. Stylianou N, Lehman ML, Wang C, Fard AT, Rockstroh A, Fazli L, et al. A molecular portrait of epithelial–mesenchymal plasticity in prostate cancer associated with clinical outcome. Oncogene 2019;38:913–34.
18. Dudas J, Ladanyi A, Ingruber J, Steinbichler TB, Riechelmann H. Epithelial to mesenchymal transition: a mechanism that fuels cancer radio/chemoresistance. Cells 2020;9:428.
19. Moreno-Bueno G, Portillo F, Cano A. Transcriptional regulation of cell polarity in EMT and cancer. Oncogene 2008;27:6958–69.
20. Liu C, Lou W, Zhu Y, Nadiminty N, Schwartz CT, Evans CP, et al. Niclosamide inhibits androgen receptor variants expression and overcomes enzalutamide resistance in castration-resistant prostate cancer. Clin Cancer Res 2014; 20:3198–210.
21. Zhu Y, Liu C, Nadiminty N, Lou W, Tummala R, Evans CP, et al. Inhibition of ABCB1 expression overcomes acquired docetaxel resistance in prostate cancer. Mol Cancer Ther 2013;12:1829–36.
22. Sakamoto S, McCann RO, Dhir R, Kyprianou N. Talin1 promotes tumor invasion and metastasis via focal adhesion signaling and anoikis resistance. Cancer Res 2010;70:1885–95.
23. Palanisamy N, Yang J, Shepherd PDA, Li-Ning-Tapia EM, Labanca E, Manyam GC, et al. The MD Anderson prostate cancer patient-derived xenograft series (MDA PCa PDX) captures the molecular landscape of prostate cancer and facilitates marker-driven therapy development. Clin Cancer Res 2020;26:4933–46.
24. Murtagh F, Legendre P. Ward's hierarchical agglomerative clustering method: which algorithms implement ward's criterion? J Classif 2014;31:274–95.
25. Benjamini Y, Hochberg Y. Controlling the false discovery rate: a practical and powerful approach to multiple testing. J R Stat Soc B 1995;57:289–300.
26. Livas L, Hasani S, Kyprianou N. Integrated therapeutic targeting of the prostate tumor microenvironment. Adv Exp Med Biol 2020;1296:183–98.
27. Zhu M, Kyprianou N. Role of androgens and the androgen receptor in epithelial-mesenchymal transition and invasion of prostate cancer cells. FASEB J 2010;24:769–77.
28. Singh A, Settleman J. EMT, cancer stem cells and drug resistance: an emerging axis of evil in the war on cancer. Oncogene 2010;29:4741–51.
29. Gravdal K, Halvosten OJ, Haukaas SA, Akslen LA. A switch from E-cadherin to N-cadherin expression indicates epithelial to mesenchymal transition and is of strong and independent importance for the progression of prostate cancer. Clin Cancer Res 2007;13:7003–11.
30. Tanaka H, Kono E, Tran CP, Miyazaki H, Yamashiro J, Shimomura T, et al. Monoclonal antibody targeting of N-cadherin inhibits prostate cancer growth, metastasis and castration resistance. Nat Med 2010;16:1414–20.
31. Jennbacken K, Tesan T, Wang W, Gustavsson H, Damber JE, Welen K. N-cadherin increases after androgen deprivation and is associated with metastasis in prostate cancer. Endocr Relat Cancer 2010;17:469–79.
32. Beer TM, Goldman B, Synold TW, Ryan CW, Vasist LS, Van Veldhuizen PJ Jr, et al. Southwest oncology group phase II study of ispinesib in androgen-independent prostate cancer previously treated with taxanes. Clin Genitourin Cancer 2008;6:103–9.
33. de Morrée E, van Soest R, Aghai A, de Ridder C, de Bruijn P, Ghobadi Moghaddam-Helmantel I, et al. Understanding taxanes in prostate cancer; importance of intratumoral drug accumulation. Prostate 2016;76:927–36.
34. de Morrée ES, Böttcher R, van Soest RJ, Aghai A, de Ridder CM, Gibson AA, et al. Loss of SLCO1B3 drives taxane resistance in prostate cancer. Br J Cancer 2016;115:674–81.
35. Mout L, de Wit R, Sturrman D, Verhoef E, Mathijssen R, de Ridder C, et al. Testosterone diminishes cabazitaxel efficacy and intratumoral accumulation in a prostate cancer xenograft model. EBioMedicine 2018;27:182–6.
36. van Soest RJ, van Royen ME, de Morrée ES, Moll JM, Teubel W, Wiemer EAC, et al. Cross-resistance between taxanes and new hormonal agents abiraterone and enzalutamide may affect drug sequence choices in metastatic castration-resistant prostate cancer. Eur J Cancer 2013;49:3821–30.
37. Kushwaha PP, Verma SS, Shankar E, Lin S, Gupta S. Role of solute carrier transporters SLC25A17 and SLC27A6 in acquired resistance to enzalutamide in castration-resistant. Mol Carcinog 2022;61:397–407.
38. McDonnell TJ, Troncoso P, Brisbay SM, Logothetis C, Chung LW, Hsieh JT, et al. Expression of the protooncogene bcl-2 in the prostate and its association with emergence of androgen-independent prostate cancer. Cancer Res 1992; 52:6940–4.
39. Haldar S, Basu A, Croce CM. Bcl2 is the guardian of microtubule integrity. Cancer Res 1997;57:229–33.
40. Scatena CD, Stewart ZA, Mays D, Tang LJ, Keefer CJ, Leach SD, et al. Mitotic phosphorylation of Bcl-2 during normal cell cycle progression and Taxol-induced growth arrest. J Biol Chem 1998;273:30777–84.
41. Ruiz de Porras V, Wang XC, Palomero L, Marin-Aguilera M, Solé-Blanch C, Indacochea A, et al. Taxane-induced attenuation of the CXCR2/BCL-2 axis sensitizes prostate cancer to platinum-based treatment. Eur Urol 2021;79: 722–33.
42. Pilling AB, Hwang C. Targeting prosurvival BCL2 signaling through Akt blockade sensitizes castration-resistant prostate cancer cells to enzalutamide. Prostate 2019;79:1347–59.
43. Seigneur E, Wang J, Dai J, Polepalli J, Südhof TC. Cerebellin-2 regulates a serotonergic dorsal raphe circuit that controls compulsive behaviors. Mol Psychiatry 2021;26:7509–21.
44. Yun SJ, Kim SK, Kim J, Cha EJ, Kim JS, Kim SJ, et al. Transcriptomic features of primary prostate cancer and their prognostic relevance to castration-resistant prostate cancer. Oncotarget 2017;8:114845–55.
45. Ylitalo EB, Thysell E, Thellenberg-Karlsson C, Lundholm M, Widmark A, Bergh A, et al. Marked response to cabazitaxel in prostate cancer xenografts expressing androgen receptor variant 7 and reversion of acquired resistance by anti-androgens. Prostate 2020;80:214–24.
46. Wang EL, Zhang J-J, Luo F-M, Fu M-Y, Li D, Peng J, et al. Cerebellin-2 promotes endothelial-mesenchymal transition in hypoxic pulmonary hypertension rats by activating NF-κB/HIF-1α/twist1 pathway. Life Sci 2023;328:121879.
47. Nguyen PL, Ma J, Chavarro JE, Freedman ML, Lis R, Fedele G, et al. Fatty acid synthase polymorphisms, tumor expression, body mass index, prostate cancer risk, and survival. J Clin Oncol 2010;28:3958–64.
48. Hanahan D. Hallmarks of cancer: new dimensions. Cancer Discov 2022;12: 31–46.
49. Su Y-C, Feng Y-H, Wu H-T, Huang Y-S, Tung C-L, Wu P, et al. Elovl6 is a negative clinical predictor for liver cancer and knockdown of Elovl6 reduces murine liver cancer progression. Sci Rep 2018;8:6586.
50. Feng YH, Chen WY, Kuo YH, Tung CL, Tsao CJ, Shiau AL, et al. Elovl6 is a poor prognostic predictor in breast cancer. Oncol Lett 2016;12:207–12.

51. Marien E, Meister M, Muley T, Gomez Del Pulgar T, Derua R, Spraggins JM, et al. Phospholipid profiling identifies acyl chain elongation as a ubiquitous trait and potential target for the treatment of lung squamous cell carcinoma. Oncotarget 2016;7:12582–97.
52. Centenera MM, Scott JS, Machiels J, Nassar ZD, Miller DC, Zinonos I, et al. ELOVL5 is a critical and targetable fatty acid elongase in prostate cancer. Cancer Res 2021;81:1704–18.
53. Tolkach Y, Merseburger A, Herrmann T, Kuczyk M, Serth J, Imkamp F. Signatures of adverse pathological features, androgen insensitivity and metastatic potential in prostate cancer. Anticancer Res 2015;35:5443–51.
54. Tamura K, Makino A, Hullin-Matsuda F, Kobayashi T, Furihata M, Chung S, et al. Novel lipogenic enzyme ELOVL7 is involved in prostate cancer growth through saturated long-chain fatty acid metabolism. Cancer Res 2009;69:8133–40.
55. Jiang L, Xiao L, Sugiura H, Huang X, Ali A, Kuro-o M, et al. Metabolic reprogramming during TGFβ1-induced epithelial-to-mesenchymal transition. Oncogene 2015;34:3908–16.
56. Kang H, Kim H, Lee S, Youn H, Youn B. Role of metabolic reprogramming in Epithelial¯Mesenchymal transition (EMT). Int J Mol Sci 2019;20:2042.
57. Li K, Guo Y, Yang X, Zhang Z, Zhang C, Xu Y. ELF5-mediated AR activation regulates prostate cancer progression. Sci Rep 2017;7:42759.
58. Yao B, Zhao J, Li Y, Li H, Hu Z, Pan P, et al. Elf5 inhibits TGF-β-driven epithelial-mesenchymal transition in prostate cancer by repressing SMAD3 activation. Prostate 2015;75:872–82.
59. Deng S, Wang C, Wang Y, Xu Y, Li X, Johnson NA, et al. Ectopic JAK-STAT activation enables the transition to a stem-like and multilineage state conferring AR-targeted therapy resistance. Nat Cancer 2022;3:1071–87.
60. Pomerantz MM, Qiu X, Zhu Y, Takeda DY, Pan W, Baca SC, et al. Prostate cancer reactivates developmental epigenomic programs during metastatic progression. Nat Genet 2020;52:790–9.
61. Davies A, Nouruzi S, Ganguli D, Namekawa T, Thaper D, Linder S, et al. An androgen receptor switch underlies lineage infidelity in treatment-resistant prostate cancer. Nat Cell Biol 2021;23:1023–34.